Science in China Series G: Physics, Mechanics & Astronomy

www.scichina.com
phys.scichina.com
www.springerlink.com

Minor alloying behavior in bulk metallic glasses and high-entropy alloys

ZHANG Yong†, ZHOU YunJun, HUI XiDong, WANG MeiLing & CHEN GuoLiang

State Key Laboratory for Advanced Metals and Materials, University of Science and Technology Beijing, Beijing 100083, China

The effect of minor alloying on several bulk metallic glasses and high-entropy alloys was studied. It was found that minor Nb addition can optimize the interface structure between the W fiber and the Zr-based bulk metallic glass in the composites, and improve the mechanical properties. Minor Y addition can destabilize the crystalline phases by inducing lattice distortion as a result to improve the glass-forming ability, and the lattice distortion energy is closely related to the efficiency of space filling of the competing crystalline phases. A long-period ordered structure can precipitate in the Mg-based bulk metallic glass by yttrium alloying. For the high-entropy alloys, solid solution can be formed by alloying, and its mechanical properties can be comparable to most of the bulk metallic glasses.

bulk metallic glasses, high-entropy alloys, solid solution, lattice distortion, entropy of mixing, glass forming ability

Bulk metallic glasses and high-entropy alloys are recently developed materials which have the potential to be the next generation of structural materials. However, before the engineering applications, some basic problems should be solved, e.g. the critical size of the bulk metallic glasses should be increased and the larger the better; the room temperature ductility should be improved; the phase formation rules of the high-entropy alloys should be systematically studied. Minor alloying is an effective method for tailoring the structures, both nano-structure and micro-structure, and moreover to improve the properties. In this paper, some examples are presented.

1 Effect of Nb addition on W fiber/Zr-based bulk metallic glass composites

The room temperature ductility of the bulk metallic glasses can be improved by preparing the tungsten fibers Zr-based metallic glass composite[1]. However, the interface reaction will weaken the strength and the ductility of tungsten and metallic glasses.

Figure 1 is the interface morphology in W fiber/$Zr_{55}Al_{10}Ni_5Cu_{30}$ matrix composite, and some

Received April 2, 2007; accepted January 9, 2008
doi: 10.1007/s11433-008-0050-5
†Corresponding author (email: drzhangy@skl.ustb.edu.cn)

interface reactant can be observed. By X-ray diffraction patterns analysis, the reactant is characterized to be W_5Zr_3 phase, which is the resultant of interface peritectic reaction between Zr in matrix and W fiber during the process of melt infiltration casting:

$$Zr(L) + W(S) \xrightarrow{\text{Peritectic reaction}} W_5Zr_3$$

This kind of peritectic reaction can not only seriously damage the properties of W fiber, but also lower the glass-forming ability (GFA) of matrix, and finally do great harm to the properties of bulk metallic glass composites.

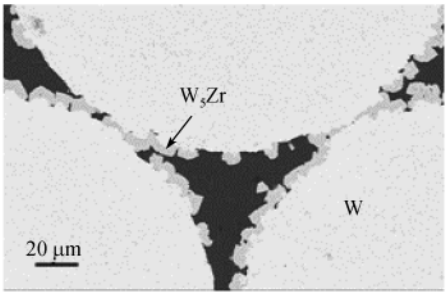

Figure 1 The interface morphology in W fiber/$Zr_{55}Al_{10}Ni_5Cu_{30}$ matrix composite.

Figure 2 is the interface morphology in Nb-containing W fiber/$Zr_{55}Al_{10}Ni_5Cu_{30}$ matrix composite. Clearly, no obvious interfacial reaction can be observed in the interface between W fibers and the matrix. So it is evident that minor Nb addition effectively restrains the harmful interface reaction during the process of melt infiltration casting.

The reason why Nb addition can optimize the interface structure in W fiber/Zr-based bulk metallic glass composites is that the alloy element Nb with a strong affinity for W prefers to segregate at the interface during casting, which can reduce the segregation and diffusion of Zr in W fiber[2].

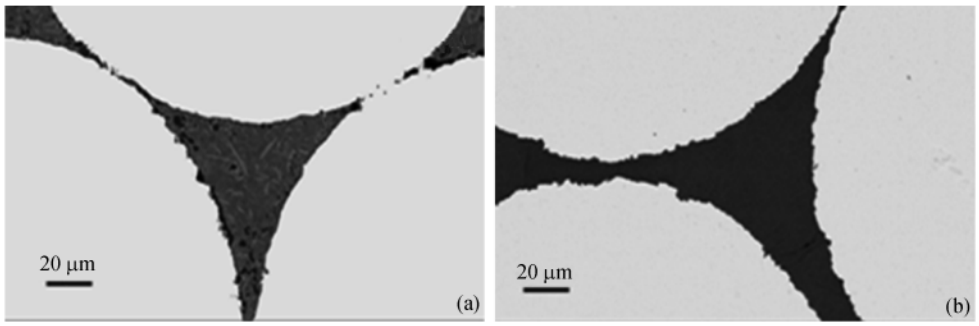

Figure 2 The interface morphology in Nb-containing composite. (a) $(Zr_{55}Al_{10}Ni_5Cu_{30})_{0.98}$ Nb_2; (b) $Zr_{57}Al_{10}Nb_5Cu_{15.4}Ni_{12.6}$.

W fiber/$Zr_{47}Ti_{13}Cu_{11}Ni_{10}Be_{16}Nb_3$ bulk metallic glass composites have the best interface structure in this study. The composite exhibits very high strength of 2.6 GPa and plastic strain of 13.5% with volume percent of tungsten of 70%, as shown in Figure 3.

2 Effect of minor Y addition on the glass-forming ability of metallic alloys

Yttrium has been widely used in some alloys as a minor addition element to improve the GFA[3,4].

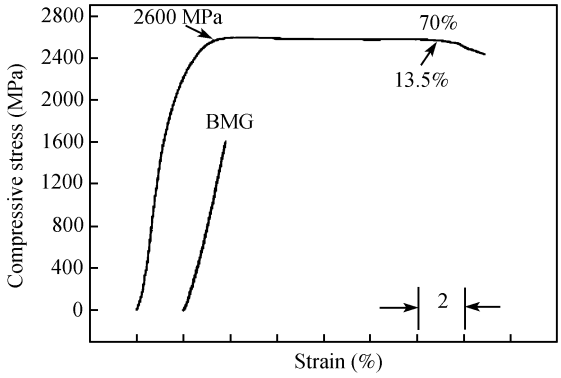

Figure 3 Stress-strain curve for compression testing of W/$Zr_{47}Ti_{13}Cu_{11}Ni_{10}Be_{16}Nb_3$ composite.

From the X-ray diffraction patterns as shown in Figure 4, a small amount of Y can effectively improve the glass-forming ability of both $Cu_{48}Zr_{48}Al_4$ and $Ti_{40}Zr_{25}Be_{20}Cu_{12}Ni_3$ alloys.

Figure 5 shows the stress-strain curves of Cu-based alloys. The alloy without yttrium addition exhibits distinct plastic elongation of 6.92%, while the alloy with 2 at.% yttrium addition exhibits 0.39% plastic strain. The Y addition makes ε_p (plastic strain limit), σ_{max} (compressive strength) and ε_e (elastic strain limit) decrease, and E (Young's modulus) and σ_y (yield strength) increase slightly.

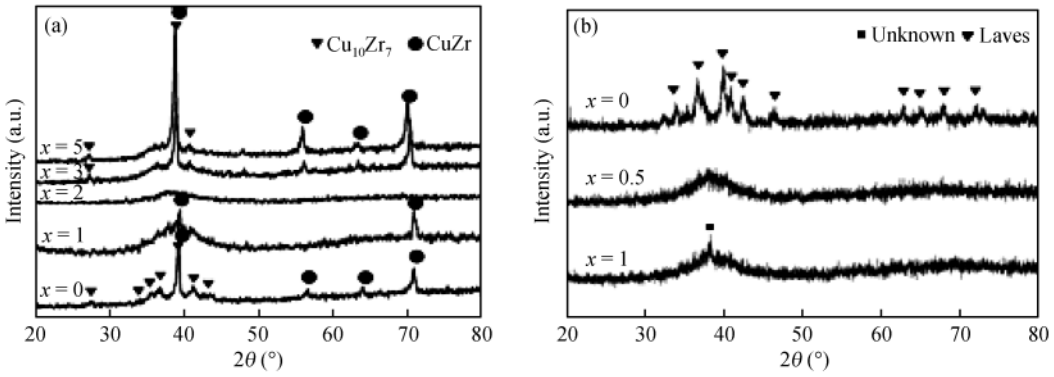

Figure 4 X-ray diffraction patterns for $(Cu_{0.48}Zr_{0.48}Al_{0.04})_{100-x}Y_x$ alloy[5] (a) and $(Ti_{0.4}Zr_{0.25}Be_{0.2}Cu_{0.12}Ni_{0.03})_{100-x}Y_x$ alloy[6] (b).

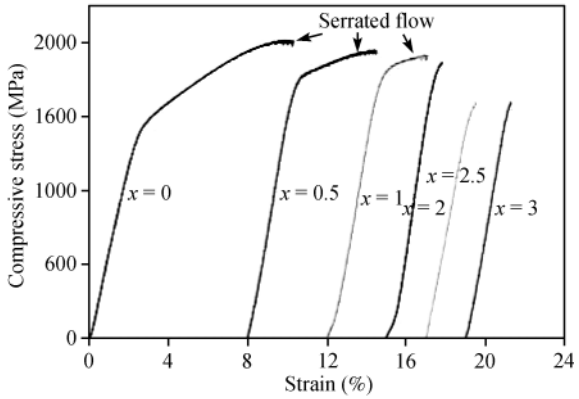

Figure 5 Stress-strain curves for compression testing of $(Cu_{0.48}Zr_{0.48}Al_{0.04})_{100-x}Y_x$ alloys[5].

Before the end of the stress-strain curves of the alloys (x = 0, 0.5, 1), the apparent serrated flow can be observed. The stress fluctuation is the distinct evidence of the formation and propagation of multiple shear bands.

The lattice distortion energy (atomic scale strain energy) is closely related to the crystal stability in the present system. As shown in Figure 6, for $(Cu_{0.48}Zr_{0.48}Al_{0.04})_{100-x}Y_x$ alloys, the efficiency of space filling is $D(Cu_{10}Zr_7) > D(CuZr)$, and thus the effective yttrium addition is $x(Cu_{10}Zr_7) < x(CuZr)$[7]. Figure 7 shows the effective addition content as a function of competing crystal efficiency of space filling, which indicates that the effective yttrium addition contents have a rough correlation with the efficiency of space filling of the easily precipitated crystal phases.

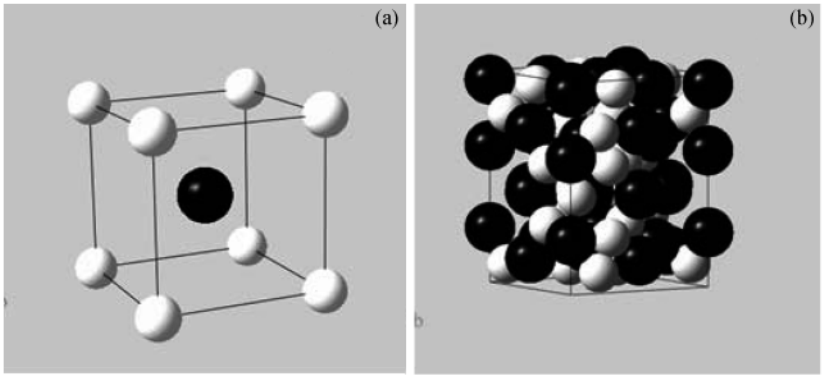

Figure 6 The crystal structures of competing crystalline phases. (a) CuZr, CsCl type, B_2 structure; (b) $Cu_{10}Zr_7$, $Ni_{10}Zr_7$ type. Here the black spheres denote Zr atoms, while the grey ones denote Cu atoms.

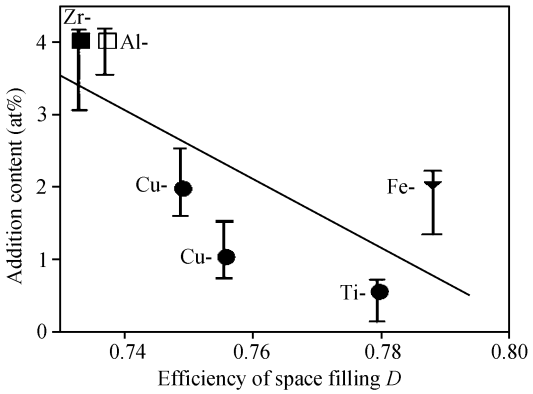

Figure 7 Dependence of effective rare earth addition content on crystal efficiency of space filling D observed in some bulk metallic glasses.

It is assumed that chemical effects between the solvent and solute (addition) atoms do not influence the location of the solute atom and, therefore, the Gibbs free energy change will be equal to the difference of lattice distortion energy induced by Y substituting Zr. Figure 8 illustrates the change of Gibbs free energy of the alloy with yttrium addition. With yttrium addition, the Gibbs free energy of the crystal would increase, and then the crystal phase is destabilized.

In $(Cu_{0.48}Zr_{0.48}Al_{0.04})_{98}Y_2$ alloys, the negative heat of mixing (HM) among Y-Cu and Zr-Cu is –22 and –23 kJ/mol, respectively, indicating that HM of Y-Cu and Zr-Cu is very close. Therefore,

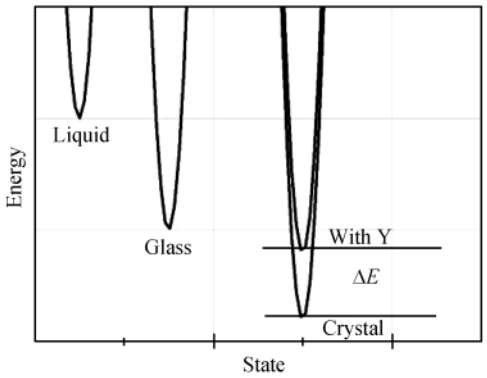

Figure 8 Illustration of the change of free energy of the crystal with yttrium addition.

considering the factors of HM and atomic size, Y may substitute the larger atoms of Zr in CuZr and $Cu_{10}Zr_7$, thus increasing the crystal cell size and inducing the lattice distortion. By taking the crystal distortion energy into account, the crystal stability would decrease, and then the glass-forming ability would increase.

3 Mg-based bulk metallic glass composites with long-period ordered structure

Mg-based bulk metallic glasses have fairly low density and very high specific strength, but the reported plasticity of Mg-based bulk metallic glasses is still under 4%[8].

Figure 9 is XRD patterns of as-cast $Mg_{65+x}(Cu_{0.667}Y_{0.333})_{30-x}Zn_5$ composite rods. For the alloy at $x = 6$, there is a broad diffraction peak between $2\theta = 30-45°$, which is the characteristic of amorphous structure. While for other composite alloys, diffraction peaks are found to superpose on the diffuse maximum of amorphous phase. The precipitates are identified as hcp Mg-based solid solution.

Figure 10 is the TEM micrographs and energy-dispersive X-ray (EDX) pattern. In the pattern as shown in Figure 10(c), extra weak spots appear regularly along the c^*-direction, which is different from the standard electron diffraction pattern of pure Mg with 2H-hcp structure, but is an

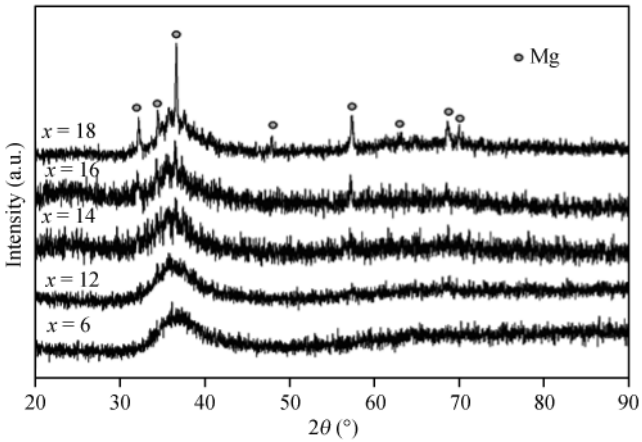

Figure 9 XRD patterns of as-cast $Mg_{65+x}(Cu_{0.667}Y_{0.333})_{30-x}Zn_5$ (x = 6, 12, 14, 16 and 18) rods with a diameter of 3 mm.

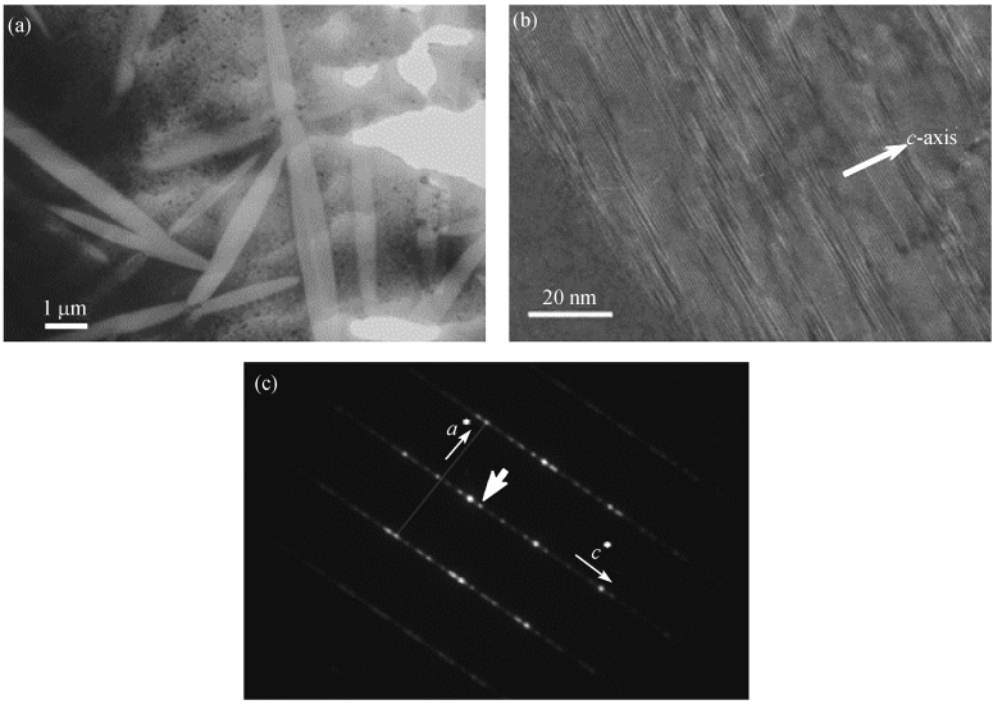

Figure 10 (a) Bright field TEM micrograph of $Mg_{81}Cu_{9.3}Y_{4.7}Zn_5$ bulk metallic glass matrix composite; (b) magnified TEM image of the flake, in which a fine-lamellar structure was observed; (c) SAED pattern of [11 $\bar{2}$ 0] zone axis taken from the flake in the composite.

ideal hexagonal lattice of 6H-type. It is also observed that the *a**-direction and the *c**-direction are not exactly perpendicular with each other, and the angle between them is estimated to be approximately 88°.

Room-temperature compressive stress-strain curves for $Mg_{65+x}(Cu_{0.667}Y_{0.333})_{30-x}Zn_5$ alloy specimens are shown in Figure 11, and the detailed mechanical properties for the alloy system are listed in Table 1. Compared with full amorphous samples, this long-period ordered structure reinforced Mg-based bulk metallic glass composites have much higher strength, and certain plastic-

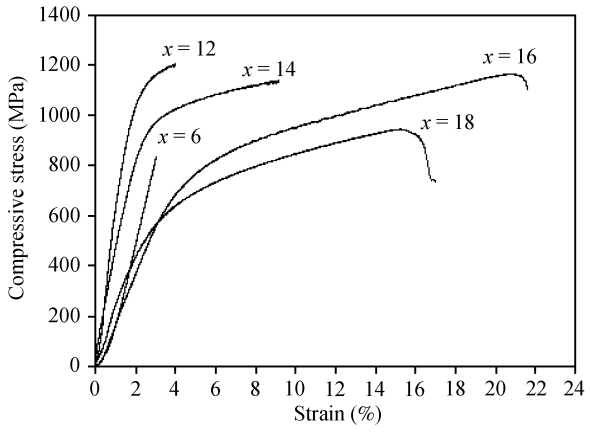

Figure 11 Room-temperature compressive stress-strain curves for $Mg_{65+x}(Cu_{0.667}Y_{0.333})_{30-x}Zn_5$ composite specimens with a diameter of 2 mm and the full glass specimen with a diameter of 3 mm ($x = 6$) at a strain rate of 10^{-4} s^{-1}.

Table 1 Detailed mechanical properties of $Mg_{65+x}(Cu_{0.667}Y_{0.333})_{30-x}Zn_5$ alloys

Sample	Yield stress σ_y (MPa)	Elastic strain ε_y (%)	Fracture strength σ_f (MPa)	Plastic strain ε_p (%)
$x = 6$	–	3.04	839	0
$x = 12$	841	1.45	1203	2.45
$x = 14$	740	1.66	1135	7.52
$x = 16$	550	2.9	1163	18.5
$x = 18$	358	1.43	942	15.4

ity at the same time. Noticeably, for $Mg_{81}Cu_{9.3}Y_{4.7}Zn_5$ alloy ($V_f = 48\%$), the composite shows fracture strength of 1163 MPa and pronounced plastic deformation of 18.5%. It is the largest value for the Mg-based BMG glass and composites reported to date. Due to its low density, the specific strength of the composite reaches 4.31×10^5 Nm/kg, which is also the highest among all reported Mg-based metallic glasses.

4 Alloying effect on high-entropy alloys

The high-entropy alloys can be defined as the alloys consisting of at least five principal elements with the concentrations of each of them being between 5 at.% and 35 at.% (near equi-atomic ratio), and according to the regular solution model, the alloys have very high entropy of mixing[9−14].

Our previous work has confirmed that certain high-entropy alloys are composed mainly of random solid solution[13]. As shown in Figure 12, when Al molar ratio is lower than 2, the alloying between Al and equi-atomic ratio TiVCrMnFeCoNiCu alloy makes the microstructure of Al_x-TiVCrMnFeCoNiCu alloys gradually become simpler. For Al_2TiVCrMnFeCoNiCu alloy, both the dendrite and interdendrite are body-centered cubic (BCC) solid solution (Figure 13).

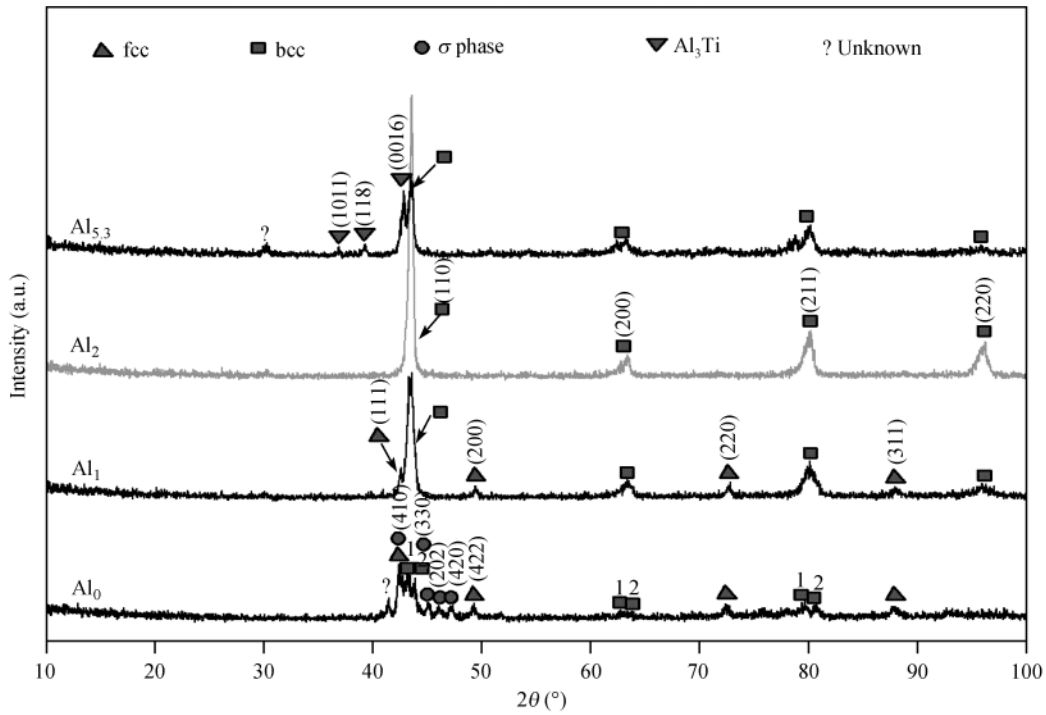

Figure 12 XRD patterns of Al_xTiVCrMnFeCoNiCu alloys.

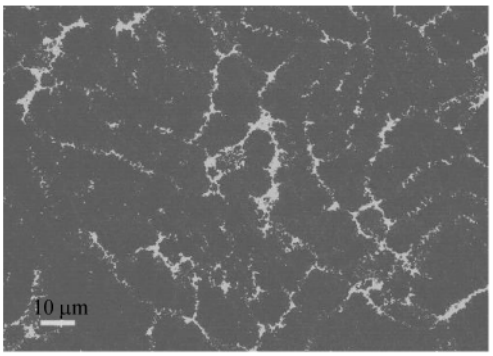

Figure 13 SEM images of $Al_2TiVCrMnFeCoNiCu$ alloy.

The superiority of simple solid solutions over intermetallic compounds in the alloys is attributed to the effect of the high mixing entropy. Following Boltzmann's hypothesis, S_{mix} of an n-element alloy is expressed as eq. (1), and would reach the maximum when the alloy is of equi-atomic ratio,

$$S_{\text{mix}} = -R\sum_{i=1}^{n} c_i \ln c_i, \tag{1}$$

where R is the gas constant, C_i the mole percent of the ith component, and $\sum_{i=1}^{n} C_i = 1$.

From eq. (1), both $Al_xTiVCrMnFeCoNiCu$ and $Ti_xCrFeCoNiCu$ alloys have very high entropy of mixing. As follows is the formula of Gibbs free energy:

$$G = H - TS. \tag{2}$$

According to eq. (2), the high entropy of the two alloy systems could significantly lower the free energy, thus lowering the tendency of being ordered, and consequently making random solid solution form more easily and more stable than ordered phases during solidification in alloys with multi-principal elements. Besides, high entropy can balance the lattice strain caused by the solid-solution phenomenon of large atom into the alloy structure, so as to make solid solution more stable than ordered intermetallics, especially at high temperature[15,16].

By components optimization, the XRD pattern and SEM images of $Ti_xCrFeCoNiAl$ alloys are shown in Figure 14. Clearly, all the four alloys are mainly composed of BCC solid solutions.

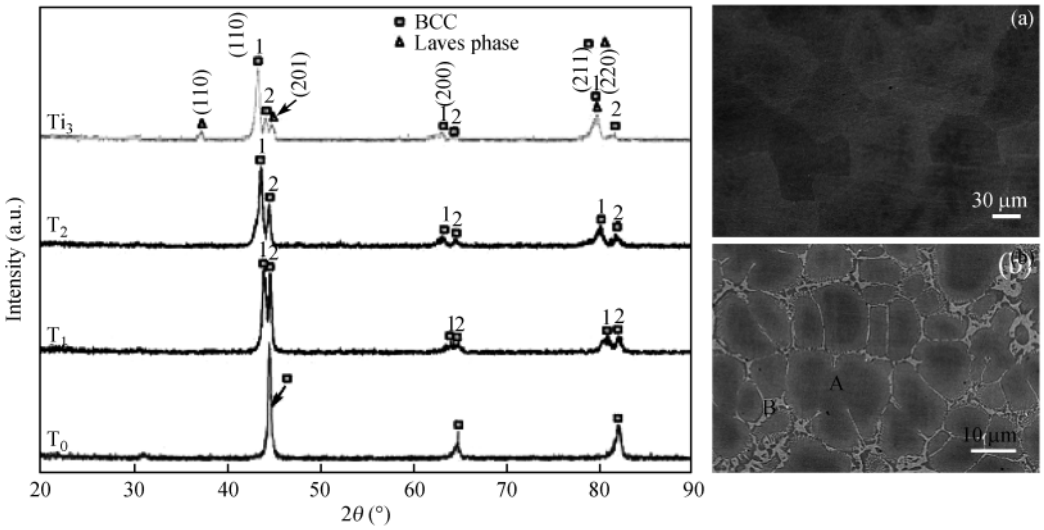

Figure 14 XRD patterns of as-cast $Ti_xCrFeCoNiAl$ alloys, and their corresponding SEM back-scattered electron images. (a) T_0 alloy; (b) T_1 alloy.

As shown in Figure 15, $Ti_xCrFeCoNiAl$ alloys have super-high strength and high plasticity. Among them, both T_0 and T_1 alloys have excellent comprehensive mechanical properties. Especially, Ti_1 alloy exhibits yield stress, fracture strength and plastic strain of 2.259 GPa, 3.135 GPa and 23.33%, respectively. It is apparent that these properties are even superior to most of the

high-strength bulk alloys reported, e.g. bulk metallic glasses.

Figure 16 is the SEM and TEM images for T_1 alloy. Clearly, the dendrites are mainly constructed

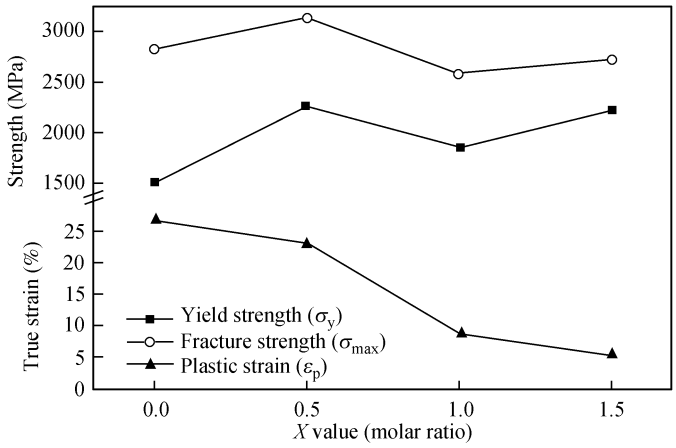

Figure 15 Room-temperature compressive mechanical properties of $Ti_xCrFeCoNiAl$ alloys.

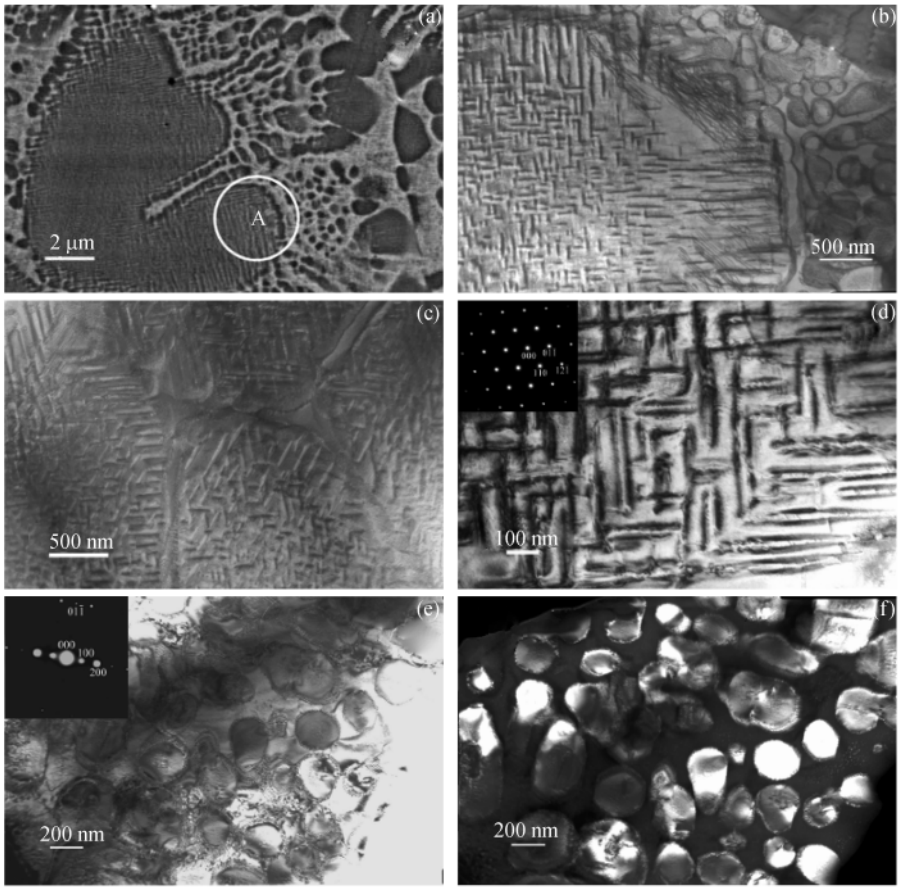

Figure 16 (a) SEM back-scattered micrograph of T_1 alloy; (b) TEM bright-field image which is corresponding to the A region marked by the circle in (a); (c) TEM bright-field image with canal-like structures; (d) bright-field image of net-like structures with SAD pattern of bcc [$\bar{1}$ 11] zone axis; (e) bright-field image of interdendrite with SAD pattern of bcc [001] zone axis; (f) dark-field image of interdendrite corresponding to the (100) superlattice spot of the SAD pattern shown in (e).

of net-like structures, which results from spinodal decomposition[16]. While in the interdendrite, a number of particles precipitate in the matrix. From TEM observation and SAD analyses, these tiny long precipitates in dendrites are characterized to be long disordered BCC Widmanstättenin phase (about 30 nm in width). It disperses in the BCC matrix, forms net-like eutectic, and provides both effective precipitation strengthening and nano-composite strengthening effects[17]. While for the particles in interdendrites, from the TEM observation and corresponding SAD analyses, they are characterized to be ordered BCC phase. It precipitates along the direction of 〈100〉, and disperses in the disordered BCC matrix. According to Orowan mechanism, these ordered particles would provide effective dispersion strengthening effect[17].

Ti_xCrFeCoNiAl alloys are mainly composed of BCC solid solution. So the solid-solution strengthening effect makes the alloy system have fairly high strength and hardness. For T_1 alloy, as Ti and Al have much larger atomic radius (1.47 Å and 1.43 Å, respectively) than other components ($\leqslant$1.28 Å[18]), they occupy the lattice sites and result in serious distorted lattice, as shown in Figure 17, so that the lattice distortion energy will be fairly high, and the effect of solid solution strengthening is enhanced, thus enabling the alloy to possess high strength[17].

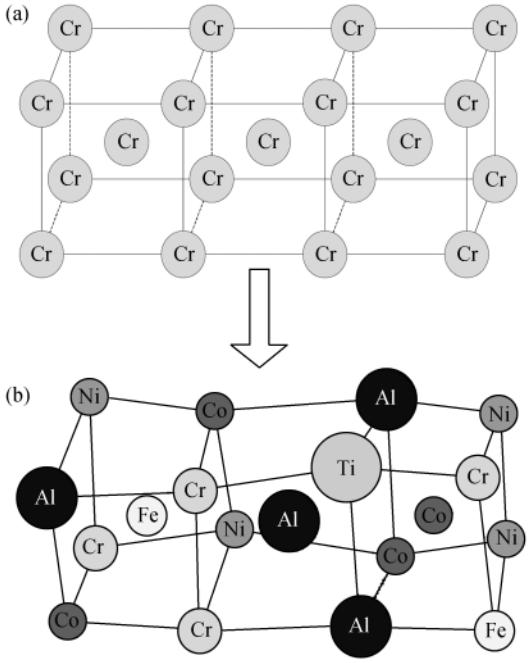

Figure 17 Schematic illustration of BCC structure. (a) Perfect lattice with the same atoms of Cr; (b) serious distorted lattice caused by many kinds of different-sized atoms randomly distributed in the crystal lattice with the same probability to occupy the lattice sites in multi-component T_1 solid solutions.

5 Conclusions

(1) Minor Nb addition can optimize the interface structure in W fiber/Zr-based bulk metallic glass composites, thus bringing about improved strength and plasticity.

(2) Minor Y addition can destabilize competing the crystalline phase in Cu- and Ti-based alloys so as to effectively improve the glass-forming ability. This effect has a close relation with the

crystal efficiency of space filling of the competing crystalline phases.

(3) By alloying, Mg-based bulk metallic glass can form long-period ordered structure composites.

(4) High-entropy alloys can form random solid solution by certain alloying, and possess the comparable mechanical properties to the bulk metallic glasses.

1 Dandliker R B, Conner R D, Johnson W L. Mechanical properties of $Zr_{57}Nb_5Al_{10}Cu_{15.4}Ni_{12.6}$ metallic matrix particulate composites. J Mater Res, 1999, 14(8): 3292

2 Wang M L, Chen G L, Hui X, et al. Optimized interface and mechanical properties of W fiber/Zr-based bulk metallic glass composites by minor Nb addition. Intermetallics, 2007, 15(10): 1309

3 Zhang Y, Pan M X, Zhao D Q, et al. Formation of Zr-based bulk metallic glasses from low purity of materials by yttrium addition. Mater Trans JIM, 2000, 41(13): 1410

4 Wang W H, Bian Z, Wen P, et al. Role of addition in formation and properties of Zr-based bulk metallic glasses. Intermetallics, 2002, 10: 1249

5 Chen J, Zhang Y, He J P, et al. Metallographic analysis of Cu-Zr-Al bulk amorphous alloys with yttrium addition. Script Mater, 2006, 54: 1351

6 Hao G J, Zhang Y, Lin J P, et al. Bulk metallic glass formation of Ti-based alloys from low purity elements. Mater Lett, 2006, 60: 1256

7 Zhang Y, Chen J, Chen G L, et al. Glass formation mechanism of minor yttrium addition in CuZrAl alloys. Appl Phys Lett, 2006, 89: 131904

8 Ma H, Xu J, Ma E. Mg-based bulk metallic glass composites with plasticity and high strength. Appl Phys Lett, 2003, 83(14): 2793

9 Greer A L. Confusion by design. Nature, 1993, 366: 303

10 Yeh J W, Chen S K, Gan J Y, et al. Formation of simple crystal structures in solid solution alloys with multiprincipal metallic elements. Metall Mater Trans, 2004, 35A: 2533

11 Wang X F, Zhang Y, Qiao Y, et al. Novel microstructure and properties of multi- component $CoCrCuFeNiTi_x$ alloys. Intermetallics, 2007, 15(3): 357

12 Zhou Y J, Zhang Y, Wang Y L, et al. Solid solution alloys of $AlCoCrFeNiTi_x$ with excellent room-temperature mechanical properties. Appl Phys Lett, 2007, 90: 181904

13 Zhou Y J, Zhang Y, Wang Y L, et al. Microstructure and compressive properties of multicomponent $Al_x(TiVCrMnFeCoNiCu)_{100-x}$ high-entropy alloys. Mater Sci Eng A, 2007, 454-455: 260

14 Yeh J W, Chen S K, Lin S J, et al. Nanostructured high-entropy alloys with multiprincipal elements-novel alloy design concepts and outcomes. Adv Eng Mater, 2004, 6: 299

15 Porter D A, Easterling K E. Phase Transformation in Metals and Alloys. New York, NY: Chapman & Hall, 1981. 308

16 De Boer F R, Boom R, Mattens W C M. Cohesion in Metals. New York, NY: Elsevier, 1988. 47

17 Harwood J J. Strengthening Mechanisms in Solids. Metals Park, Ohio: ASM Seminar, 1960. 23

18 Kittel C. Introduction to Solid State Physics. 6th ed. New York: John Wiley & Songs, Inc., 1980. 67